

# Measurement of device parameters using image recovery techniques in large-scale IC devices

Leif Scheick, Member, IEEE, Larry Edmonds

**ABSTRACT**—Devices that respond to radiation on a cell level will produce histograms showing the relative frequency of cell damage as a function of damage. The measured distribution is the convolution of distributions from radiation responses, measurement noise, and manufacturing parameters. A method of extracting device characteristics and parameters from measured distributions via mathematical and image subtraction techniques is described.

## I. INTRODUCTION

VLSI devices will exhibit a response to radiation on a cell level [1], [2], [3], [4], [5]. That is, individual cells in a device will report a total ionizing dose (TID) and/or a displacement damage response. DRAMs, SRAMs, floating gate devices such as EPROMs and Flash memories, and ASICs have all demonstrated a change in a measurable quantity. DRAMs show a change in retention time [4]. SRAMs exhibit a change in minimum operating voltage [1]. EPROMs and Flash memories demonstrate a shift in programming and erasure charge [5]. In the older (large feature size) technologies, dose coverage is effectively uniform and identical radiation exposures applied to identical devices produces nearly identical results. In contrast, the individual cells in a device of VLSI or greater density (the subject of interest here) can show varied responses to the same irradiation exposure. For a radiation source like gamma or electrons, the radiation response of identical cells may be tightly grouped because the dose coverage is effectively uniform even when viewed on a small scale [1], [2], [3]. Localized radiation, like protons and heavy ions, will cause more variance in the radiation responses [4], [5]. In the latter case, the device response is plotted either as a histogram or a probability distribution, showing the relative frequency of cell damage as a function of damage. Such a plot, whether it be a histogram or a normalized probability distribution, will be called a radiation response curve.

The issue of how dose distributes across an array of sensitive cells has been an issue for several different types of systems. Extracting and determining the parameters that influence the dose distribution has been a major focus [6]–[8]. The extraction of device parameter from distributions of microdose damage across substrates has been described [6]. Hard errors in memories are described by changing in damage distributions in [7]. Methods have also been employed to directly measure the spatial distribution of dose.

This paper shows how the radiation response curve can be equated to two numerical parameters that can be used to quantify the susceptibility of the cells to radiation damage. The parameters are also determinations of the physical parameters governing the interaction of radiation across the device. Given a radiation response curve, the two susceptibility parameters can be extracted. Conversely, if the two parameters are given, a radiation response curve can be predicted. These parameters are more directly related to the physical characteristics of a device and damage mechanisms than the radiation response curves, so de-convolving a curve into these parameters can add insight regarding physical mechanisms. These parameters depend not only on device characteristics, but also on the type of irradiation (e.g., protons versus heavy ions), so different irradiation types can be compared to each other by comparing these parameters.

The theory applies to any measure of damage that has the additive property. The additive property means that the measure of damage in a cell, accumulated from multiple particle hits, is the sum of the damage measures from each hit. The dark current in a device that responds to displacement damage is an example of such a measure of damage. Each carrier generation site created by a particle hit makes an additive contribution to the dark current, and the dark current from the collection of sites created by one particle hit is added to the dark current from the collection of sites created by another hit. In this study, the total amount of fluence is low, so the damage to the device does not saturate and is therefore linear. To emphasize the generality of the theory, the generic term “damage” will be used throughout this paper. The type of damage is arbitrary, and the units that it is expressed in are arbitrary, providing that it has the additive property [9].

## II. IMAGE SUBTRACTION

An instrumentation readout of a measure of damage will be called a signal. For example, if the damage is measured by the dark current in a cell but the instrumentation reports this as a number of mV, this number is the signal. Several sources contribute to the cell-to-cell variations in the measured signal. In addition to a distribution of radiation responses, there is also a distribution due to the variance of manufacturing parameters across the die of the device. We will call this the original distribution. A third contribution is the variance of the noise distribution inherent in the measurement techniques [10]. Each contribution adds another dimension to the analytical complexity, so it is desirable to eliminate as many as possible. The noise distribution is included in the analysis but the original distribution is not. Instead, it is removed from the measured data via the image subtraction method (explained below). In addition to analytical complexity considerations, another motivation for using image subtraction instead of other methods (such as mathematical de-convolution) is sensitivity. Image subtraction can resolve a radiation response from the original distribution with high precision even if the cell-to-cell variation associated with the original distribution is large enough to completely mask the radiation response when other methods are used. Image subtraction is the process of analyzing the change in signal at every spatial point on an image. Previous studies

<sup>1</sup> The research in this paper was carried out by the Jet Propulsion Laboratory, California Institute of Technology under contract with the National Aeronautics and Space Administration (NASA) Code AE, under the Electronic Parts and Packaging Program (NEPP).

L. Scheick is with the Jet Propulsion Laboratory, California Institute of Technology, Pasadena, CA 91109 USA (telephone: 818-354-3272, e-mail: leif.scheick@jpl.nasa.gov).

L. Edmonds is with Jet Propulsion Laboratory, California Institute of Technology, Pasadena, CA 91109 USA (telephone: 818-354-2778, e-mail: larry.edmonds@jpl.nasa.gov).

have called the result of image subtraction the “shift spectrum” [1]. If the signal of each cell is measured prior to irradiation, and then measured again after irradiation, the signal difference at every cell can be calculated and the resulting distribution will be the convolution of the radiation response distribution and the noise distribution. If the second measurement was done without irradiation, i.e., if two measurements are made prior to irradiation, the resulting distribution will be the noise distribution.

### III. EXPERIMENTAL DATA

The theoretical model discussed in later sections will be compared to experimental data. The data are discussed now, before the model, because this discussion also explains how the data should be processed and presented for comparison with the model.

The devices used in this study were FPA fabricated from a JPL design. The imaging array consisted of a 512 by 512 array of 3T active pixel sensors. The CMOS devices were built on a 0.6  $\mu\text{m}$  HP process. This device is completely digital, so the signal from each FPA cell is reported digitally on the output pins. This allows for temperature compensation of dark current. The peripheral circuitry sets integration time and data is clocked out synchronously with a clock input. For this study, a PC interrogated the device using a LABVIEW based code. The pixel size is 12  $\mu\text{m}$  by 12  $\mu\text{m}$  with a fill factor of 44%. The full well capacity is  $2.4 \times 10^{-14}$  C. The output range is 1.63V. The charge collection gain is the ratio of output voltage to charge collected and is 4.2  $\mu\text{V}/\text{e}$  at the photodiode. The ADC consists of a radiation hardened 10 bit 225 kHz device. The maximum data acquisition rate is 20 Mpixels/s. Therefore, the minimum integration time is equal to the frame read time or 300ms.

For this experiment, the biased device was irradiated with 60 MeV protons supplied by the Crocker Nuclear Laboratory. All irradiations occurred at normal incidence. The fixed pattern noise (FPN) and the dark current were measured between irradiation steps. The supply current and other CMOS parameters were monitored to ensure integrity of the read out circuitry. Two different integration times were also set to measure dependence on the integration time. The operating bias was set to 5 volts and the operating temperature was held at  $-25^\circ\text{C}$  throughout the study.

To establish a baseline response of the device, two dark current distributions were measured prior to irradiation. The histograms are plotted in Fig. 1. Both plots were readouts measured from the same virgin chip at different times. The abscissa of Fig. 1 is the dark rate at which each cell in the FPA reports when read. The ordinate of Fig. 1 is the number of cells that report that dark rate. Each distribution is the convolution of the original distribution and the noise distribution. The original distribution should be identical for the two measurements, but the noise distribution is not. The result is that the two measured distributions are very similar but not identical. Image subtraction was used for a precise determination of the noise distribution and the result is shown in Fig. 2. The non-zero mean of this distribution is typical of offset noise in the ADC of this device.

The device was then irradiated with protons. After each irradiation step, the signal distribution was measured and image subtraction was used to remove the original distribution. The resulting histograms are plotted in Fig. 3a. Each distribution is the convolution of the radiation response distribution and the noise distribution. The figure shows that the distribution gets wider and the mean shifts higher with increasing dose. This is typical of microdosimetric response in cell arrays [1], [2], [3], [4], [5].

In addition to removing the original distribution, image subtraction can also be used to remove prior irradiation distributions. Fig. 3b depicts the image subtraction of two consecutive irradiations, which is the convolution of the incremental irradiation and the noise. Now the fact that the image subtraction spectra for each incremental dose are not identical indicates that the sensitivity of the APS cells change with dose. The distributions are wider as dose increases, which imply that the cells are more sensitive to damage as dose increases. The measurement of the change in the sensitivity of device parameters is a primary focus of this study.

The vertical scales in the histograms in Figs. 2 and 3 depend on the arbitrarily selected signal bin size. This dependence can be removed by renormalizing the histograms so that the integral of each is 1. This normalization converts each histogram in Figs. 2 and 3a into a probability density and the results are shown in Fig. 4. The horizontal axis in the figure is an adjusted dark signal obtained by offsetting the original axis by the amount needed to center the noise distribution at zero signal. This compensates for the offset noise in the ADC of the device.

### IV. CROSS SECTION FOR INCREMENTAL DAMAGE

Having presented the experimental data in Fig. 4, the next task is to derive a model that can be compared to the data. Note that cumulative damage reflects two kinds of statistics. One describes the number of particle hits (some cells can be hit by more particles than other cells), and the other describes the damage produced by a single hit (some particle hits may be more damaging than other hits within the same cell, for reasons explained below). Both kinds of statistics can be derived from a single function, which is the cross section for the incremental damage to exceed a specified value. “Incremental damage” is defined to be the damage created by a single particle hit, so it is a single event effect. Different hits can produce different amounts of incremental damage for any combination of several reasons. One possible reason is that cell sensitivity depends on the location at which damage is created, so some hit locations are more damaging than other hit locations within the same cell. Another possible reason is that damage is caused by collision reactions that are described statistically, i.e., some hits produce a given reaction while others do not. Whatever the reason, incremental damage is a single event effect that can be described by a cross section  $\sigma(D_I)$ , which is associated with an individual cell and is the cross section for the incremental damage to exceed a specified value  $D_I$ . Note that the cross section depends not only on the selected level of damage, but also on the type (species and energy) of incident particles that the device is exposed to. The

notation does not display this dependence because the particle type is held fixed throughout the analysis.

This cross section could be experimentally defined if it is possible to record the incremental damage in each cell each time an increment of damage is created. In the absence of an actual experiment, the concept of a cross section can still be made clear by referring to a thought experiment. In this thought experiment, incremental damage is measured in a selected cell each time an increment of damage is created. We select a value for  $D_I$ , expose the cell to some fluence  $F$ , and count the number of times in which a single particle hit created a damage exceeding  $D_I$  (the fluence must be large enough to make this count large enough for good counting statistics). The cross section is this count divided by  $F$ .

The experimental definition of  $\sigma(D_I)$  is generic, i.e., does not depend on the physical mechanisms by which damage is created, but the physical interpretation of  $\sigma(D_I)$  does depend on such mechanisms. For illustration, consider a device (hypothetical if not real) in which damage is created by charge liberated by direct ionization by the incident particle. Neglecting statistical variations in the amount of liberated charge from different particle hits, the damage may still depend on the location within the cell at which the charge is liberated. In this case, the cross section  $\sigma(D_I)$  is the area of that portion of the cell in which the fixed liberated charge produces a damage exceeding  $D_I$ . For another illustration, consider a device (hypothetical if not real) in which the sensitive area of each cell is a single number in the sense that the cell sensitivity is spatially uniform within this area. Damage is created, in this example, by collision reactions that produce displacements. Displacement clusters are described statistically because some can be larger (more damaging) than others. In this case, the cross section  $\sigma(D_I)$  is the sensitive area multiplied by the probability of producing a displacement cluster that is large enough to produce a damage exceeding  $D_I$ .

Given that the damage measure has the additive property, the cross section for incremental damage implicitly contains all information regarding device susceptibility whether expressed as a function of incremental damage or cumulative damage. Numerical parameters that measure device susceptibility are obtained by fitting the cross section with a function containing adjustable parameters that are selected for a best fit. The fit selected for this analysis is given by

$$\sigma(D_I) = A e^{-B D_I} \quad (1)$$

where  $A$  and  $B$  are constants. These constants are the parameters that describe device susceptibility.  $A$  and  $B$  can be functions of  $D_I$ , but for this analysis the variation with  $D_I$  is negligible. If the actual cross section on the left does not have the functional form indicated on the right, it is still possible to define  $A$  and  $B$  parameters for any given cross section by stipulating that they be selected for a best fit. The  $A$  parameter is the saturation value of the cross section. The  $B$  parameter has two interpretations. One interpretation obtained directly from (1) is  $B=1/D_{I,1/e}$ , where  $D_{I,1/e}$  is that value of incremental damage at which the cross section is  $1/e$  times the saturation value. A second interpretation is obtained by using (1) to evaluate the integrals to obtain

$$\frac{1}{B} = \frac{\int_0^{\infty} D_I \sigma(D_I) dD_I}{\int_0^{\infty} \sigma(D_I) dD_I}$$

which can also be written as

$$B = 1/D_{I,AVG} \quad (2a)$$

where

$$D_{I,AVG} \equiv \frac{\int_0^{\infty} D_I \sigma(D_I) dD_I}{\int_0^{\infty} \sigma(D_I) dD_I} \quad (2b)$$

Note that  $D_{I,AVG}$  defined by (2b) is the weighted average incremental damage, weighted by the cross section. This is also a conditional statistical average; the average (over particle hits) incremental damage, given that the cell was hit. Stated another way, it is the average incremental (or per hit) damage that averages over a large random sampling of particles that hit the selected cell (particles that miss the cell do not add to the damage but also do not contribute to the sample size). This type of average, which averages over particles, is distinguished from another type of average that averages over cells. For example, the number of hits can be averaged over cells. The average number of hits from a fluence  $F$  is  $AF$ , and the average number of hits that produce an incremental damage that exceeds  $D_I$  is  $\sigma(D_I)F$ .

## V. MODEL PREDICTIONS

Appendix A shows how the cross section for incremental damage is used to construct a probability distribution for cumulative damage. The appendix also shows how the latter distribution is combined with a noise distribution to obtain the measured probability distribution, denoted here as  $\rho_M$ . The final results from the appendix are summarized here, without the derivations, in the form of a plotting recipe. This recipe plots model predictions in the format of Fig. 4, i.e., different curves correspond to different fluences and each curve plots  $\rho_M$  as a function of  $D$ . The recipe requires numerical values for the  $A$  and  $B$  parameters. If the objective is to fit an existing curve, for which these parameters are not known in advance, trial values are assigned. The best values are those that produce the best fit. The equations indicated in the recipe are in Appendix A. The protocol is as follows:

- Step 1:** It is assumed that the noise distribution has already been measured. Assign a numerical value to the parameter  $C$  in (14).
- Step 2:** Assign numerical values to the parameters  $A$  and  $B$ .
- Step 3:** Different curves are characterized by different values of  $F$ . Select a particular curve by assigning a numerical value to  $F$ .
- Step 4:** Calculate  $\mu_p$  from (13a) and then  $S_p^2$  from (13b).
- Step 5:** Calculate  $K_1$  and then  $K_2$  from (19).
- Step 6:** Select an entry from the table in Appendix B. Each entry produces another point to be plotted. Use the selected entry to assign numerical values to  $z$  and  $G$ .
- Step 7:** Calculate  $D'$  from  $D' = z^2 / (ABF)$ . Then calculate  $D$  from  $D = (D' - K_2) / K_1$ .

**Step 8:** Calculate  $\rho_N(D)$  from (14) and then calculate  $\rho_M$  from (18a). Plot the point  $(D, \rho_M)$ .

**Step 9:** Repeat Steps 6 through 8 for additional points on the selected  $F$  curve.

The above recipe was used to obtain curves to be compared to those in Fig. 4. In Step 1, setting the amplitude  $C$  of the fitting function equal to the peak value (0.7/mV) of the measured noise curve gives an excellent fit. Trial values were assigned in Step 2 and those that gave adequate fits to the measured curves in Fig. 4 were recorded. The results are shown in Fig. 5. The first irradiation, irrad 1, was not sufficiently distinctive from noise to successfully extract the  $A$  and  $B$  parameters. That is, when noise is deconvolve from the irrad 1 data set, the result does not give and measurable  $A$  or  $B$  parameter. This inability sets the lower bound of the method, which is the signal distribution must be appreciably above the noise distribution. The  $A$  and  $B$  parameters are indicated in each plot and compared in Table I.

Table I: Extracted parameters from deconvolution

Fluence [1/cm <sup>2</sup> ]	A [cm <sup>2</sup> ]	B [1/mV]
$5.0 \times 10^{10}$	$1.4 \times 10^{-10}$	3.4
$7.5 \times 10^{10}$	$1.9 \times 10^{-10}$	3.4
$12.5 \times 10^{10}$	$2.4 \times 10^{-10}$	3.4

The parameter  $A$  increases with dose while the parameter  $B$  does not change with dose. It was expected from the analysis of Fig. 3b that one of the parameters  $A$  or  $B$  would change with dose. As can be seen from Table 1, the change in  $A$  is small with dose. This variation is judged to be small enough to conclude that the model is in reasonable agreement with the data. Good fits are obtained by using a common  $B$  for all plots but there is some variation in  $A$  from one plot to the next.

## VI. DISCUSSION

The model and techniques discussed here allows us to estimate two device parameters that would otherwise be obscured in measured data containing noise and an original distribution in addition to a radiation response distribution. One parameter is the average per-hit damage (averaged over particle hits), which is  $1/B$ . From Fig. 5 or Table I we estimate this to be about 0.3 mV for the example considered. The other parameter is the effective sensitive area of a cell, which is  $A$ . The term “effective” is used because a physical area might be multiplied by a collision reaction probability if collision reactions produce the damage (displacement damage). If the damage is caused by direct ionization from the incident particle (micro-dose),  $A$  is expected to be some physical area. The exact value of  $A$  depends on which plot is selected from Fig. 5, but in any case it is between 0.01 and 0.03  $\mu\text{m}^2$  for the example considered. This is very much smaller than a pixel area ( $12\mu\text{m} \times 12\mu\text{m}$  with a 44% fill factor), suggesting that the damage was caused by collision reactions.

The credibility of the above assertion can be tested by comparing the values of  $A$  in Table I to an estimate obtained from an independent analysis derived from the stated assertion. This analysis follows earlier work by Srour *et al.* [7]. Those

authors found that leakage currents produced by displacement damage are quantized, so the occurrence or nonoccurrence of detectable damage is unambiguous. Each silicon atom in the sensitive volume has a cross section for a collision that ultimately leads to detectable damage. The cross section used in [7] for 99 MeV protons was 4.2 barns ( $4.2 \times 10^{-24} \text{ cm}^2$ ). The same per-atom cross section is used here for 60 MeV protons for order-of-magnitude estimates. The parameter  $A$  is the cell cross section for obtaining any amount of detectable damage and is the above per-atom cross section multiplied by the number of silicon atoms in the sensitive volume. The area of the volume is  $0.44 \times 12\mu\text{m} \times 12\mu\text{m}$  and the depth (depletion region thickness of a fully depleted pixel) is 10  $\mu\text{m}$ , giving a volume of  $6.3 \times 10^{-10} \text{ cm}^3$ . Multiplying by  $5 \times 10^{22} \text{ atoms/cm}^3$  and then multiplying by the per-atom cross section produces the estimate  $A \approx 1.3 \times 10^{-10} \text{ cm}^2$ . This order-of-magnitude estimate agrees with the values listed in Table I, so the assertion that damage is caused by collision reactions is consistent with the measured data.

## VII. CONCLUSIONS

The response of an array to microdose inducing radiation can be determined using a mathematical model combined with image subtraction. Device and radiation effect parameters can be extracted by using this method. In particular, image subtraction has sufficient resolution to produce the curves in Fig. 4 in spite of the large spread in the original histograms such as shown in Fig. 1. Furthermore, applying the mathematical model to Fig. 4 leads to the conclusion that the data are consistent with the assertion that damage is caused by collision reactions (displacement damage).

## APPENDIX A: DERIVATION

### A. Radiation Response

We start with the radiation response alone, i.e., noise is not included in this part of the analysis. Let  $P(D, F)$  denote the probability that a selected cell will receive a cumulative (i.e., summed over particle hits) damage  $D$  when exposed to a fluence  $F$ . The term “exceeds” is a strict inequality, so  $P(0, F)$  is not 1. Instead, it is the probability that the cell was hit somewhere at least once. The cross section for incremental damage is given by (1) with a saturation value equal to  $A$ , so the probability that the cell was hit somewhere (i.e., the area  $A$  was hit) one or more times is given (via Poisson statistics) by

$$P(0, F) = 1 - e^{-AF}. \quad (3a)$$

There is zero probability that the damage will exceed zero or any larger value if the fluence is zero, so another boundary condition is

$$P(D, 0) = 0. \quad (3b)$$

The two boundary conditions in (3) join continuously at the point  $D=0, F=0$ , so  $P(D, F)$  will be a smooth function. This is the motivation for interpreting “exceeds” as a strict inequality; to make  $P(D, F)$  a smooth function. The penalty is that  $P(D, F)$  does not satisfy the traditional normalization condition (i.e.,  $P(0, F) \neq 1$ ) because it does not include all possibilities. It does not include the possibility of no hits, which has a probability

of  $1-P(0,F)=e^{-AF}$ , so this possibility has to be included as a separate term in the analysis.

An equation governing  $P(D,F)$  can be derived by selecting a fluence value  $F$  and an additional fluence increment  $\Delta F$ . The probability  $P(D,F+\Delta F)$  can be expressed in terms of conditional probabilities according to

$$P(D,F+\Delta F)=[1-P(0,F)]P_{cond}(D,F+\Delta F|0,F)+\int_{0+}^{\infty}\rho(D',F)P_{cond}(D,F+\Delta F|D',F)dD' \quad (4)$$

where the symbols are explained below. The square bracket on the right side of (4) is the probability of zero damage (no hits) when the fluence is  $F$ , and the term that multiplies it is a conditional probability; the probability that the damage will exceed  $D$  when the fluence is  $F+\Delta F$ , given that there was no damage when the fluence was  $F$ . The term  $\rho(D',F)$  is the probability density for the damage to be  $D'$  when the fluence is  $F$ , and the term that multiplies it is a conditional probability; the probability that the damage will exceed  $D$  when the fluence is  $F+\Delta F$ , given that the damage was exactly  $D'$  when the fluence was  $F$ . The square bracket is  $e^{-AF}$ , and  $\rho$  is given by

$$\rho(D,F)=-\frac{\partial P(D,F)}{\partial D}. \quad (5)$$

Elementary probability theory can calculate the two conditional probabilities to first order in  $\Delta F$  (i.e., in the limit of small  $\Delta F$ ) in terms of the cross section for incremental damage, and the results are

$$P_{cond}(D,F+\Delta F|0,F)\approx\sigma(D)\Delta F$$

$$P_{cond}(D,F+\Delta F|D',F)\approx\sigma(D-D')\Delta F \quad \text{if } D>D'$$

$$P_{cond}(D,F+\Delta F|D',F)=1 \quad \text{if } D'>D$$

which become exact in the limit of small  $\Delta F$ . Substituting these results into (4) gives

$$P(D,F+\Delta F)-P(D,F)=e^{-AF}\sigma(D)\Delta F$$

$$-\int_0^D\sigma(D-D')\frac{\partial P(D',F)}{\partial D'}dD'\Delta F.$$

Dividing by  $\Delta F$  and taking the limit as  $\Delta F\rightarrow 0$  gives

$$\frac{\partial P(D,F)}{\partial F}=e^{-AF}\sigma(D)-\int_0^D\sigma(D-D')\frac{\partial P(D',F)}{\partial D'}dD'.$$

This equation can be expressed in terms of  $\rho$  defined by (5) by differentiating to get

$$\frac{\partial\rho(D,F)}{\partial F}=e^{-AF}\sigma_{diff}(D)-\sigma(0)\rho(D,F)$$

$$+\int_0^D\sigma_{diff}(D-D')\rho(D',F)dD' \quad (6)$$

where  $\sigma_{diff}$  is the differential cross section defined by

$$\sigma_{diff}(D)\equiv-\frac{d\sigma(D)}{dD}. \quad (7)$$

The equation governing  $\rho$  is put in its final form by combining (1) with (6) and (7) to get

$$\frac{\partial\rho(D,F)}{\partial F}+A\rho(D,F)=ABe^{-(AF+BD)}$$

$$+ABe^{-BD}\int_0^De^{BD'}\rho(D',F)dD'. \quad (8)$$

Expressing the boundary conditions (3) in terms of  $\rho$  gives

$$\int_0^{\infty}\rho(D,F)dD=1-e^{-AF}, \quad \rho(D,0)=0. \quad (9)$$

The solution to (8) and (9) is

$$\rho(D,F)=ABFe^{-(BD+AF)}\sum_{k=0}^{\infty}\frac{(ABDF)^k}{k!(k+1)!} \quad (10)$$

which can be verified by substituting the proposed solution into (8) and (9). It is convenient to define the function  $G$  by

$$G(z)\equiv e^{-2z}\sum_{k=0}^{\infty}\frac{z^{2k}}{k!(k+1)!} \quad (11)$$

so (10) can be written as

$$\rho(D,F)=ABFe^{-(\sqrt{BD}-\sqrt{AF})^2}G(\sqrt{ABDF}). \quad (12)$$

This is more convenient than (10) because  $G$  varies much more slowly than the series in (10), so a tabulation of  $G$  can be prepared in advance and then interpolated for each application. A tabulation is given in Appendix B. For the benefit of readers that want to make their own tables, some properties of the series in (11) are stated here without proof. If the infinite series is approximated by summing all terms up to some finite number of terms, the relative (or fractional) error is bounded by the first omitted term. For example, an error of not greater than 1% is insured if the terms are summed until the first encounter of a term that is less than 0.01. Numerical problems (computer overflow) can occur if  $z$  is very large but an asymptotic expression can be used for such cases. This is

$$G(z)\rightarrow\frac{1}{2z\sqrt{\pi z}} \quad (\text{large } z)$$

which gives three-digit accuracy when  $z=300$ , with better accuracy at larger  $z$ . The series (11) is recommended for  $z<300$ .

Using (10) to evaluate the required integrals will show that the mean of  $\rho$ , denoted  $\mu_\rho$ , and variance of  $\rho$ , denoted  $S_\rho^2$ , are given by

$$\mu_\rho\equiv\frac{\int_0^{\infty}D\rho(D,F)dD}{\int_0^{\infty}\rho(D,F)dD}=\frac{1}{1-e^{-AF}}\frac{AF}{B} \quad (13a)$$

$$S_\rho^2\equiv\frac{\int_0^{\infty}(D-\mu_\rho)^2\rho(D,F)dD}{\int_0^{\infty}\rho(D,F)dD}=\frac{1}{1-e^{-AF}}\frac{(AF)^2+2AF}{B^2}-\left(\frac{1}{1-e^{-AF}}\frac{AF}{B}\right)^2. \quad (13b)$$

## B. Noise

The radiation response probability density  $\rho$  is now combined with a noise probability density denoted  $\rho_N$  to obtain a measured probability density denoted  $\rho_M$ . The noise distribution is fit with a Gaussian function given by

$$\rho_N(D)=Ce^{-\pi C^2D^2} \quad (14)$$

where  $C$  is a constant. The required normalization is built into (14), so there is only one adjustable fitting parameter  $C$ , which was arbitrarily selected to be the amplitude. The mean

and variance of  $\rho$  are denoted  $\mu_N$  and  $S_N^2$  (respectively) and are given by

$$\mu_N = 0, \quad S_N^2 = 1/(2\pi C^2). \quad (15)$$

By starting with conditional probabilities in analogy with (4) we can obtain

$$\rho_M(D, F) = e^{-AF} \rho_N(D) + [1 - e^{-AF}] \int_0^\infty \frac{\rho(D', F)}{1 - e^{-AF}} \rho_N(D - D') dD'. \quad (16)$$

The square bracket was factored out of the integral in (16) so that the integral will be the convolution between two distributions that are normalized in the traditional way. The integral can be evaluated exactly but the result is extremely messy. An alternative is to replace the integral with an approximation. Assuming that the fluence  $F$  is large enough to make the radiation distribution clearly distinguishable from the noise distribution, the noise distribution is treated as a small perturbation in the sense that the  $\rho_N$  in the integral is a narrow pulse. The convolution will then resemble the distribution  $\rho/[1 - e^{-AF}]$ , but slightly altered to have the increased spread or variance created by the noise. We therefore use the approximation

$$\int_0^\infty \frac{\rho(D', F)}{1 - e^{-AF}} \rho_N(D - D') dD' \approx \frac{K_1 \rho(K_1 D + K_2, F)}{1 - e^{-AF}} \quad (17)$$

where the constants  $K_1$  and  $K_2$  are selected for a best fit, as discussed later. Using (17) together with (12), we can write (16) as

$$\rho_M(D, F) \approx e^{-AF} \rho_N(D) + K_1 A B F e^{-(\sqrt{B D'} - \sqrt{A F})^2} G(z) \quad (18a)$$

where

$$D' \equiv K_1 D + K_2, \quad z \equiv \sqrt{A B D' F}. \quad (18b)$$

There still remains the task of selecting  $K_1$  and  $K_2$ . The objective is to make the right side of (17) have the same normalization, mean, and variance as the left side. The left side is the convolution between two normalized distributions, and a well-known property of such a convolution is that it is normalized, has a mean equal to the sum of the two means ( $\mu_\rho + \mu_N = \mu_\rho$ ), and has a variance equal to the sum of the two variances ( $S_\rho^2 + S_N^2 = S_\rho^2 + 1/(2\pi C^2)$ ). The right side of (17) already has the required normalization, so  $K_1$  and  $K_2$  are selected to give the right side a mean equal to  $\mu_\rho$  and a variance equal to  $S_\rho^2 + 1/(2\pi C^2)$ . It is easy to show that the required values are given by

$$K_1 = \left[ \frac{S_\rho^2}{S_\rho^2 + 1/(2\pi C^2)} \right]^{1/2}, \quad K_2 = (1 - K_1) \mu_\rho. \quad (19)$$

#### APPENDIX B: TABULATION OF G

$z$	$G(z)$	$z$	$G(z)$
0	1	9.0	1.023e-2
0.02	9.610e-1	9.5	9.441e-3
0.04	9.239e-1	10	8.751e-3
0.06	8.885e-1	11	7.599e-3
0.08	8.549e-1	12	6.679e-3

0.10	8.228e-1	13	5.931e-3
0.20	6.838e-1	14	5.312e-3
0.30	5.739e-1	15	4.794e-3
0.40	4.862e-1	16	4.356e-3
0.50	4.158e-1	17	3.980e-3
0.60	3.588e-1	18	3.655e-3
0.70	3.122e-1	19	3.372e-3
0.80	2.738e-1	20	3.124e-3
0.90	2.419e-1	21	2.905e-3
1.0	2.153e-1	22	2.710e-3
1.2	1.737e-1	23	2.536e-3
1.4	1.434e-1	24	2.380e-3
1.6	1.206e-1	25	2.240e-3
1.8	1.031e-1	26	2.112e-3
2.0	8.938e-2	27	1.997e-3
2.2	7.839e-2	28	1.891e-3
2.4	6.945e-2	29	1.795e-3
2.6	6.207e-2	30	1.706e-3
2.8	5.590e-2	31	1.624e-3
3.0	5.068e-2	32	1.549e-3
3.2	4.623e-2	33	1.480e-3
3.4	4.238e-2	34	1.415e-3
3.6	3.904e-2	35	1.355e-3
3.8	3.611e-2	36	1.299e-3
4.0	3.354e-2	37	1.247e-3
4.2	3.125e-2	38	1.198e-3
4.4	2.921e-2	39	1.153e-3
4.6	2.738e-2	40	1.110e-3
4.8	2.574e-2	41	1.070e-3
5.0	2.425e-2	42	1.032e-3
5.2	2.290e-2	43	9.961e-4
5.4	2.168e-2	44	9.624e-4
5.6	2.055e-2	45	9.306e-4
5.8	1.952e-2	46	9.005e-4
6.0	1.858e-2	47	8.720e-4
6.2	1.771e-2	48	8.449e-4
6.4	1.690e-2	49	8.193e-4
6.6	1.615e-2	50	7.949e-4
6.8	1.549e-2	60	6.051e-4
7.0	1.481e-2	75	4.332e-4
7.2	1.421e-2	94	3.089e-4
7.4	1.365e-2	120	2.143e-4
7.6	1.312e-2	150	1.534e-4
7.8	1.263e-2	190	1.076e-4
8.0	1.217e-2	240	7.581e-5
8.5	1.113e-2	300	5.426e-5

#### REFERENCES

- [1] Scheick, L.Z.; Swift, G.M.; Dose and microdose measurement based on threshold shifts in MOSFET arrays in commercial SRAMs Nuclear Science, IEEE Transactions on , Volume: 49 Issue: 6 , Dec 2002 Page(s): 2810 -2817
- [2] Xapxos, M.A.; Freitag, R.K.; Burke, E.A.; Dozier, C.M.; Brown, D.B.; Summers, G.P.; The random nature of energy deposition in gate oxides Nuclear Science, IEEE Transactions on , Volume: 36 , Issue: 6 , Dec. 1989 Pages:1896 - 1903
- [3] Poivey, C.; Carriere, T.; Beaucour, J.; Oldham, T.R.; Characterization of single hard errors (SHE) in 1 M-bit SRAMs from single ion Nuclear Science, IEEE Transactions on , Volume: 41 , Issue: 6 , Dec 1994 Pages:2235 - 2239
- [4] Scheick, L.Z.; Guertin, S.M.; Swift, G.M.; Analysis of radiation effects on individual DRAM cells Nuclear Science, IEEE Transactions on Volume: 47 , Issue: 6 , Dec. 2000 Pages:2534 - 2538
- [5] Cellere, G.; Pellati, P.; Chimenton, A.; Wyss, J.; Modelli, A.; Larcher, L.; Paccagnella, A.; Radiation effects on floating-gate memory cells Nuclear Science, IEEE Transactions on , Volume: 48 , Issue: 6 , Dec. 2001 Pages:2222 - 2228

- [6] M. A. Xapsos, R. K. Freitag, C. M. Dozier, D. B. Brown, G. P. Summers, E. A. Burke, and P. Shapiro, "Separation of radiation induced and process induced later non-uniformities," *IEEE Trans. Nucl. Sci.*, vol. 37, no. 6, pp. 1677-1683, Dec. 1990.
- [7] C. Dufour, P. Garnier, T. Carriere, J. Beaucour, R. Ecoffet, M. Labrunce, "Heavy ion induced single hard errors on submicronic memories," *IEEE Trans. Nucl. Sci.*, vol. 39, no. 6, pp. 1693-1697, Dec. 1992.
- [8] E. Takada, K. Sugiyama, H. Takahashi, T. Iguchi, M. Nakazawa, "Neutron radiation distribution sensor using Flexible scintillating fiber counting with the time-of-flight technique," *IEEE Trans. Nucl. Sci.*, vol. 42, no. 4, pp. 507-511, Dec. 1995.
- [9] J.R. Srour, R.A. Hartmann, and K.S. Kitazaki, "Permanent Damage Produced by single proton interactions in silicon devices," *IEEE Trans. Nucl. Sci.*, vol. 33, no. 6, pp. 1597-1604, Dec. 1986.
- [10] Bogaerts, J., Dierickx, B., Mertens, R., "Enhanced dark current generation in proton-irradiated CMOS active pixel Sensors", *Nuclear Science, IEEE Transactions on*, Volume: 49 Issue: 3, Jun 2002, Page(s): 1513 -1521

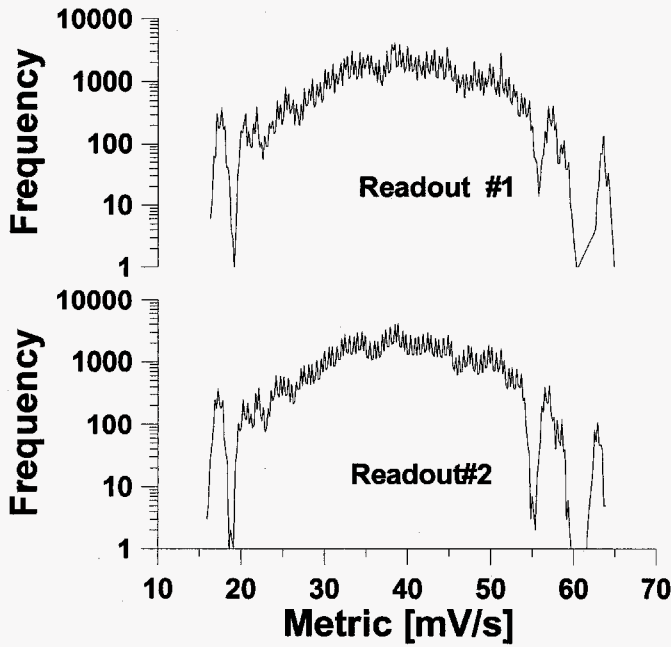


Fig. 1. Original distribution of dark signal across the FPA for two readouts of virgin devices.

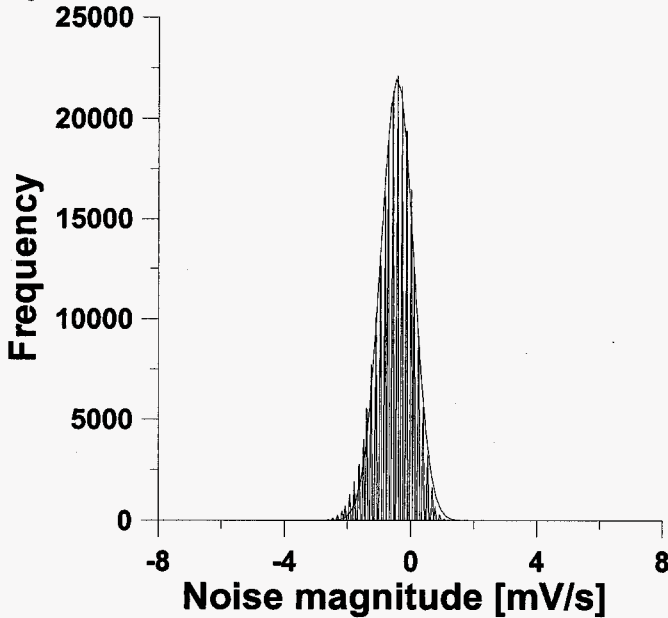


Fig. 2. Image subtraction, or shift spectra, showing the noise distribution.

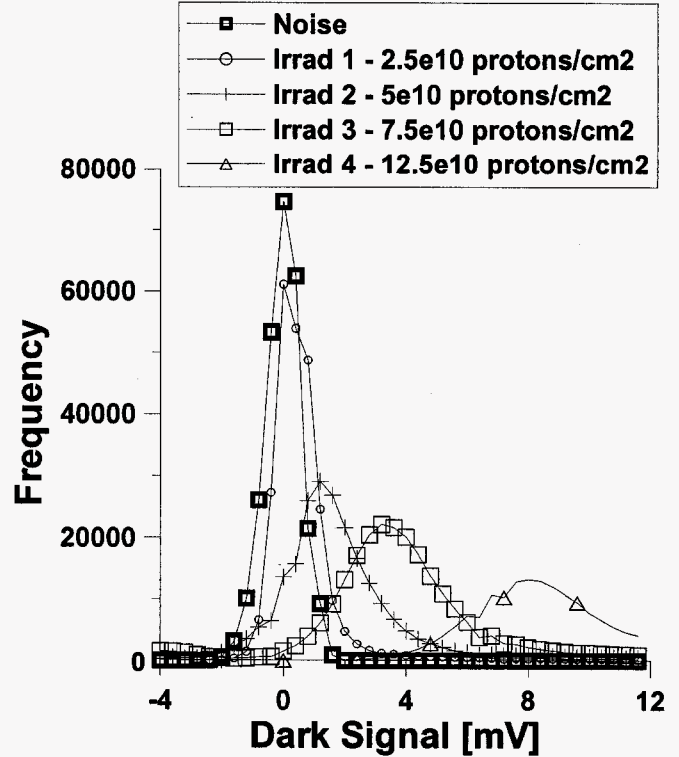


Fig. 3a. Histograms showing the damage distributions after each of several proton irradiations. Image subtraction removed the original distribution so each of the above are convolutions of the radiation response distributions with the noise distribution.

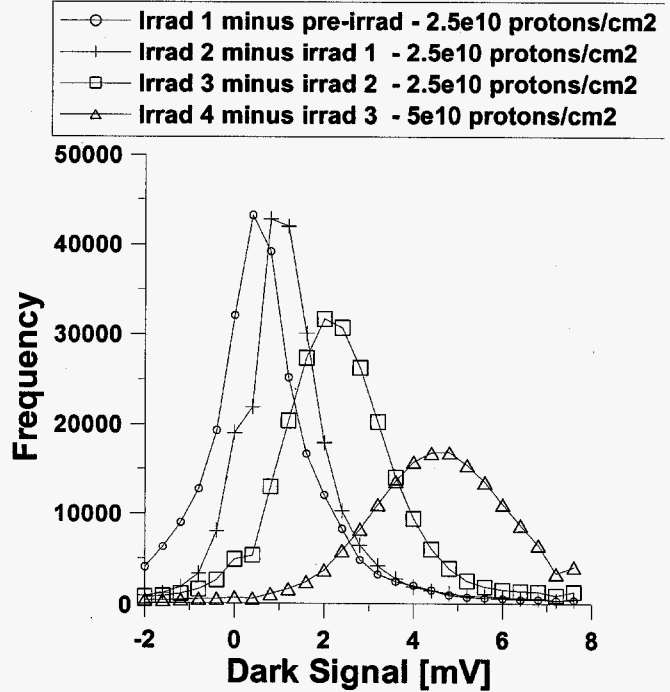


Fig. 3b. Histograms showing the damage distributions between each of several proton irradiations. Image subtraction is used to compare the damage for each dosing.

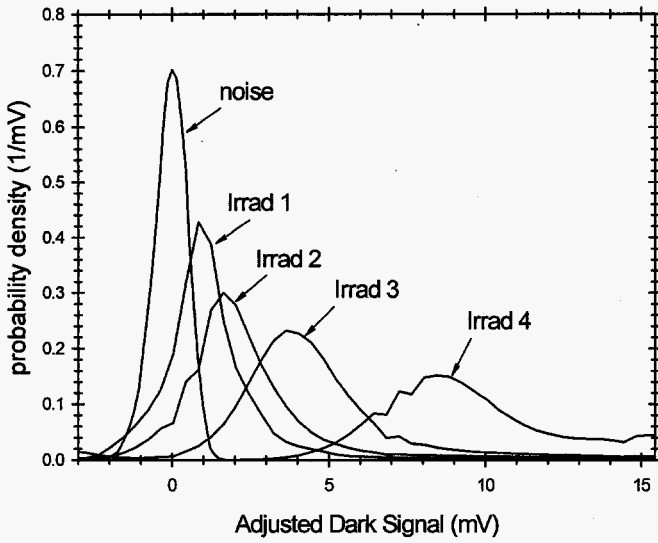


Fig. 4. A renormalization applied to the histograms in Figs. 2 and 3a produces the probability densities shown. The adjusted dark signal compensates for the offset noise in the ADC.

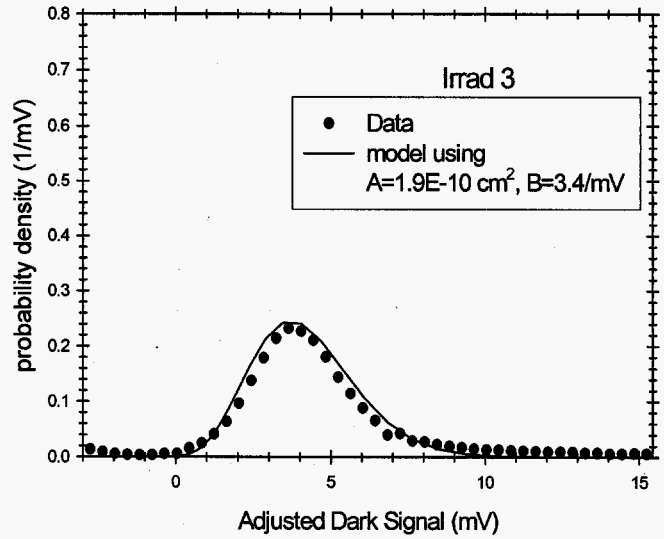


Fig. 5b. The model is compared to data obtained after the third irradiation ( $7.5E10$  protons/cm<sup>2</sup>).

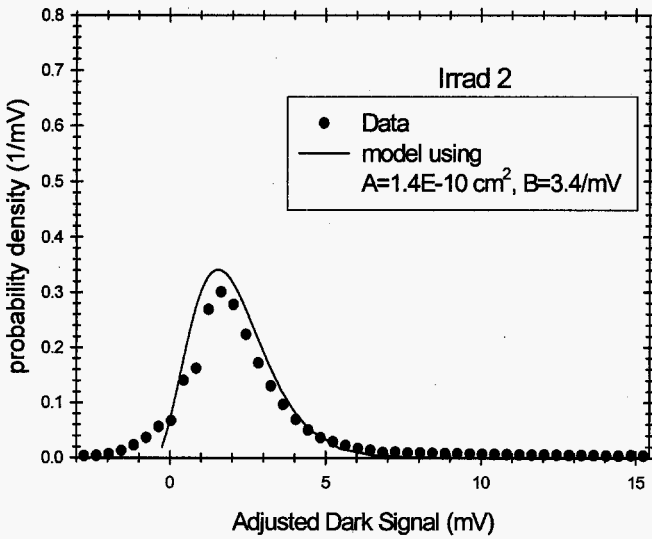


Fig. 5a. The model is compared to data obtained after the second irradiation ( $5.0E10$  protons/cm<sup>2</sup>).

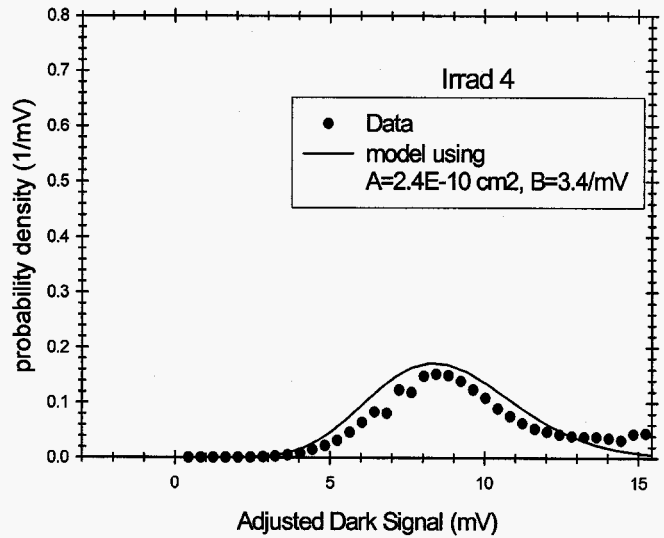


Fig. 5c. The model is compared to data obtained after the fourth irradiation ( $12.5E10$  protons/cm<sup>2</sup>).

End of File

